Path Design for Portable Access Point in Joint Sensing and Communications under Energy Constraints

Xiaoye Jing[1], Fan Liu[2] and Christos Masouros[1]
[1]University College London, London WC1E 7JE, UK
[2]Southern University of Science and Technology, Shenzhen 518055, China
Email: x.jing@ucl.ac.uk, liuf6@sustech.edu.cn, chris.masouros@ieee.org

***Abstract*—We consider an unmanned aerial vehicle (UAV) based joint radar localization and communication system, where a UAV transmits the downlink signal to a ground communication user and the transmitted signal is also exploited to localize a target coordinates. We aim to optimize the UAV path with energy constraints. We formulate the trajectory design into a weighted optimization problem, where a scalable performance trade-off between localization and communication can be achieved. An iterative algorithm is exploited then to address the trajectory design formulation. Numerical results are provided to validate the effectiveness of the proposed UAV trajectory design approaches.**

***Index Terms*—Cramér-Rao bound, joint sensing and communication, convex optimization**

I. Introduction

The joint radar localization and communication systems allow the reuse of hardware for both localization and communication functionalities, and are recognised as a key technology for reducing the hardware cost in next generation wireless systems [1]. Since unmanned aerial vehicle (UAV) network can provide flexible topology and on demand connectivity in many emergency situations, it is an important component in future wireless systems [2]. By jointly designing localization and communication in one UAV network, which can achieve a significant decrease of the payload of UAV and an improvement of the UAV network flexibility.

The research in UAV based wireless networks can be classified into two categories, namely, static UAV deployment and moving UAV trajectory design. For static UAVs, the UAV location can be designed to sense the target location related measurements, i.e., azimuth angle and distance [3]. The researches in UAV communication systems focus on the UAV coverage performance determined by the single UAV's altitude [4], [5] and topology methods of multi-UAV deployment [6], [7]. Comparing with static UAVs, moving UAVs can provide a more flexible UAV service. In regard to radar localization, the single UAV path [8] and multi-UAV paths [9] are designed for target localization and tracking. In the communication side, energy-efficient UAV communication design has received considerable attentions [10], [11].

There are some existing UAV based joint radar localization and communication researches. In [12], a power allocation scheme was proposed in a multi-UAV deployment to maximize the utility performance for communication and radar sensing.

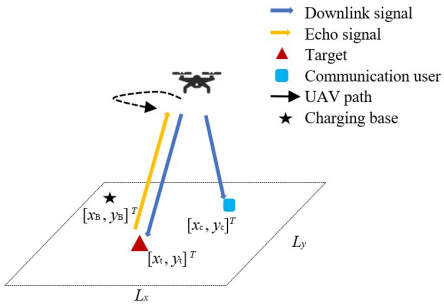

Fig. 1. Rotary-wing UAV based joint localization and communication system

In [13], a single UAV trajectory design was proposed. The UAV service strategy was designed to sense multi-user and transmit the fresh sensing data to the base station.

These current studies of UAV based joint localization and communication only consider the UAV energy consumption related to transmission. In practice, the UAV energy consumed via flying and hovering is the main energy consumption. In this paper, we consider a UAV based joint localization and communication with energy constraints. We assume that the UAV provides downlink communication for a communication user and performs radar sensing for a target using the same signal. The joint performance improvement problem is formulated into a trade-off trajectory design problem. An iterative algorithm based on successive convex approximation (SCA) is exploited for this problem.

II. System Model

In Fig. 1, one rotary-wing UAV flies in a given rectangular area. The communication user and the target are located as $[x_\mathrm{c}, y_\mathrm{c}]^T$ and $[x_\mathrm{t}, y_\mathrm{t}]^T$, respectively. The UAV flies with a fixed altitude H and the designed flying path is described by a matrix $\mathbf{S} = [\mathbf{s}_1, ..., \mathbf{s}_n, ..., \mathbf{s}_N] \in \mathbb{R}^{2\times N}$, where $\mathbf{s}_n \in \mathbb{R}^{2\times 1}$, is the waypoint of the UAV path. The flying path between two continuous waypoints is a line segment, with a constant velocity denoted as

$$\mathbf{v}_n = (\mathbf{s}_n - \mathbf{s}_{n-1}) / T_\mathrm{f}, \tag{1}$$

where T_f is the flying duration. We set a matrix $\mathbf{V} = [\mathbf{v}_1, ..., \mathbf{v}_n, ..., \mathbf{v}_N]$ to denote UAV flying velocities.

Meanwhile, the UAV hovers at several points in the designed path and performs radar sensing for a ground target. There are K hovering points, denoted by two vectors $\mathbf{x} = [x_1, ..., x_k, ..., x_K]^T$ and $\mathbf{y} = [y_1, ..., y_k, ..., y_K]^T$. The k-th hovering point is $[x_k, y_k]^T$. Specifically, after the UAV flies over $M-1$ waypoints (M is a given integer), it hovers at the next waypoint with a duration T_{h} to perform one-time sensing, so that $K = \mathrm{floor}\left(\frac{N}{M}\right)$. The k-th hovering point is

$$[x_k, y_k]^T = \mathbf{s}_{k \cdot M}, k = 1, 2, ..., K. \tag{2}$$

The downlink signal is used to transmit data to the communication user continuously when it flies following the designed path. Simultaneously, at each hovering point, the downlink signal reflected by the target is received by the UAV. Using time delay between the downlink signal and its echo, the distance between the k-th hovering point and the target is estimated. Finally, distance measurements are applied together to realize target localization.

The free-space path loss model is applicable to both communication and radar sensing. The signal-to-noise ratio (SNR) from the UAV to the user can be expressed as

$$SNR_{\mathrm{c}}(n) = \frac{P \cdot \alpha_0}{\sigma_0^2 \left[d_{\mathrm{c}}(n)\right]^2}, n = 1, 2, ..., N, \tag{3}$$

where P is the transmit power. σ_0^2 is the noise power at the receiver. α_0 is the channel power at the reference distance $d_{\mathrm{c}}(n) = 1\mathrm{m}$, where $\|\mathbf{s}_n - [x_{\mathrm{c}}, y_{\mathrm{c}}]^T\| = d_{\mathrm{c}}(n)$.

We assume that $\|\mathbf{s}_{n-1} - \mathbf{s}_n\| \ll H$. Therefore, the distance between the UAV to the communication user when the UAV flies between $\mathbf{s}_{n-1}$ and $\mathbf{s}_n$ is approximately unchanged. Therefore, the UAV average downlink data rate can be expressed as

$$\overline{R}(\mathbf{S}) = \frac{1}{N} \sum_{n=1}^{N} B \log_2 \left(1 + \frac{P \cdot \alpha_0}{\sigma_0^2 \left[d_{\mathrm{c}}(n)\right]^2}\right). \tag{4}$$

For target localization, the target location $[x_{\mathrm{t}}, y_{\mathrm{t}}]^T$ is determined by at least 3 different distance measurements, which indicates that at least $K = 3$. In the radar sensing model, $d_{\mathrm{s}}(k)$ is the distance from the UAV to the target, which is

$$d_{\mathrm{s}}(k) = \sqrt{H^2 + \| [x_k, y_k]^T - [x_{\mathrm{t}}, y_{\mathrm{t}}]^T \|^2}. \tag{5}$$

We represent the distance between the target and all hovering points as a vector $\mathbf{d}_{\mathrm{s}} = [d_{\mathrm{s}}(1), ..., d_{\mathrm{s}}(K)]^T$. $d_{\mathrm{s}}(k)$ is

$$\widehat{d}_{\mathrm{s}}(k) = d_{\mathrm{s}}(k) + w_d(k), \tag{6}$$

where $w_d(k)$ denotes the measurement Gaussian noise with zero mean and variance of σ_k^2. Let $\widehat{\mathbf{d}}_{\mathrm{s}} = \left[\widehat{d}_{\mathrm{s}}(1), ..., \widehat{d}_{\mathrm{s}}(k), ..., \widehat{d}_{\mathrm{s}}(K)\right]^T$. Note that σ_k^2 is subject to individual Gaussian distribution, which is inversely proportional to the received SNR of the echo [14].

The two-way channel power gain from $[x_k, y_k]^T$ to $[x_{\mathrm{t}}, y_{\mathrm{t}}]^T$ plus from $[x_{\mathrm{t}}, y_{\mathrm{t}}]^T$ to $[x_k, y_k]^T$ is

$$g_k = \sqrt{\frac{\beta_0}{\left[d_{\mathrm{s}}(k)\right]^4}}, \tag{7}$$

where β_0 is the channel power at the reference distance $d_{\mathrm{s}}(k) = 1\mathrm{m}$. Thus, the received echo at $[x_k, y_k]^T$ is

$$SNR_{\mathrm{s}}(k) = \frac{P \cdot G_{\mathrm{p}} \cdot g_k^2}{\sigma_0^2} = \frac{P \cdot G_{\mathrm{p}} \cdot \beta_0}{\sigma_0^2 \left[d_{\mathrm{s}}(k)\right]^4} \tag{8}$$

where G_{p} is the signal processing gain. So that we remark

$$\sigma_k^2 = a \times \frac{\sigma_0^2 \left[d_{\mathrm{s}}(k)\right]^4}{P G_{\mathrm{p}} \beta_0}, \tag{9}$$

where a is pre-determined constant related to the system.

In the target localization problem, let $\mathbf{u} = [x_{\mathrm{t}}, y_{\mathrm{t}}]^T$ and $\widehat{\mathbf{u}} = [\widehat{x}_{\mathrm{t}}, \widehat{x}_{\mathrm{t}}]^T$ is the estimation of $\mathbf{u}$. Since mean squared error (MSE) is difficult to calculate in a closed-form and accordingly the minimization of MSE is almost intractable, we employ the Cramér-Rao bound (CRB) which provides a lower bound for MSE [15], [16] as localization evaluation.

Thus, the CRB of x_{t} and y_{t} is calculated. First, we obtain the CRB matrix of $\mathbf{u}$, which is denoted as

$$\mathrm{CRB}_{\mathbf{u}} = \mathbf{J}^{-1}(\mathbf{u}), \tag{10}$$

where $\mathbf{J}(\mathbf{u})$ is the Fisher's information matrix (FIM) of $\mathbf{u}$. The FIM with respect to $\mathbf{d}_{\mathrm{s}}$ is attained easily, so we can first construct the FIM with $\mathbf{d}_{\mathrm{s}}$ and exploit the mathematical relationship between $\mathbf{d}_{\mathrm{s}}$ and $\mathbf{u}$ to derive the FIM with $\mathbf{u}$ [15].

From (6) and (9), we observe that both $\widehat{d}_{\mathrm{s}}(k)$ and σ_k^2 are depended on $d_{\mathrm{s}}(k)$. Thus the measurement vector $\widehat{\mathbf{d}}_{\mathrm{s}}$ and its covariance matrix $\mathbf{C}(\mathbf{d}_{\mathrm{s}})$ are

$$\widehat{\mathbf{d}}_{\mathrm{s}} \sim \mathcal{N}(\mathbf{d}_{\mathrm{s}}, \mathbf{C}(\boldsymbol{d}_{\mathrm{s}})), \tag{11}$$

$$\mathbf{C}(\mathbf{d}_{\mathrm{s}}) = \frac{a\sigma_0^2}{P G_{\mathrm{p}} \beta_0} \mathrm{diag}\left(\left[d_{\mathrm{s}}(1)\right]^4, \left[d_{\mathrm{s}}(2)\right]^4, ..., \left[d_{\mathrm{s}}(K)\right]^4\right). \tag{12}$$

Therefore, given by [17], the i,j-th element in the FIM of $\mathbf{d}_{\mathrm{s}}$ is shown in (13) at the top of the next page.

Then, the FIM for coordinates x_{t} and y_{t} can be derived by the chain rule in the form of

$$\mathbf{J}(\mathbf{u}) = \mathbf{Q} \mathbf{J}(\mathbf{d}_{\mathrm{s}}) \mathbf{Q}^T, \tag{14}$$

where $\mathbf{Q}$ is a Jacobian matrix in the form of

$$\mathbf{Q} = \frac{\partial \mathbf{d}_{\mathrm{s}}^T}{\partial \mathbf{u}} = \begin{bmatrix} \frac{x_1 - x_{\mathrm{t}}}{d_{\mathrm{s}}(1)} & \cdots & \frac{x_K - x_{\mathrm{t}}}{d_{\mathrm{s}}(K)} \\ \frac{y_1 - y_{\mathrm{t}}}{d_{\mathrm{s}}(1)} & \cdots & \frac{y_K - y_{\mathrm{t}}}{d_{\mathrm{s}}(K)} \end{bmatrix}. \tag{15}$$

Finally, substituting (13) and (15) into (14), $\mathbf{J}(\mathbf{u})$ is obtained and the CRB matrix of coordinates x_{t} and y_{t} is

$$\mathrm{CRB}_{\mathbf{u}} = [\mathbf{J}(\mathbf{u})]^{-1} = \frac{1}{\Theta_{\mathrm{a}} \Theta_{\mathrm{b}} - [\Theta_{\mathrm{c}}]^2} \begin{bmatrix} \Theta_{\mathrm{b}} & \Theta_{\mathrm{c}} \\ \Theta_{\mathrm{c}} & \Theta_{\mathrm{a}} \end{bmatrix}, \tag{16}$$

$$\Theta_{\mathrm{a}} = \sum_{k=1}^{K} \left\{ \frac{P G_{\mathrm{p}} \beta_0}{a \sigma_0^2} \frac{(x_k - x_{\mathrm{t}})^2}{\left[d_{\mathrm{s}}(k)\right]^6} + \frac{8 \cdot (x_k - x_{\mathrm{t}})^2}{\left[d_{\mathrm{s}}(k)\right]^4} \right\}, \tag{17}$$

$$\Theta_{\mathrm{b}} = \sum_{k=1}^{K} \left\{ \frac{P G_{\mathrm{p}} \beta_0}{a \sigma_0^2} \frac{(y_k - y_{\mathrm{t}})^2}{\left[d_{\mathrm{s}}(k)\right]^6} + \frac{8 \cdot (y_k - y_{\mathrm{t}})^2}{\left[d_{\mathrm{s}}(k)\right]^4} \right\}, \tag{18}$$

$$\Theta_{\mathrm{c}} = \sum_{k=1}^{K} \left\{ \frac{P G_{\mathrm{p}} \beta_0}{a \sigma_0^2} \times \frac{(x_k - x_{\mathrm{t}})(y_k - y_{\mathrm{t}})}{\left[d_{\mathrm{s}}(k)\right]^6} \right\} + \sum_{k=1}^{K} \left\{ \frac{8 \cdot (x_k - x_{\mathrm{t}})(y_k - y_{\mathrm{t}})}{\left[d_{\mathrm{s}}(k)\right]^4} \right\}. \tag{19}$$

$$[\mathbf{J}(\mathbf{d}_{\mathrm{s}})]_{ij}=\left[\frac{\partial \mathbf{d}_{\mathrm{s}}}{\partial d_{\mathrm{s}}(i)}\right]^{T}\mathbf{C}^{-1}(\mathbf{d}_{\mathrm{s}})\left[\frac{\partial \mathbf{d}_{\mathrm{s}}}{\partial d_{\mathrm{s}}(j)}\right]+\frac{1}{2}\mathrm{tr}\left[\mathbf{C}^{-1}(\mathbf{d}_{\mathrm{s}})\frac{\partial \mathbf{C}(\mathbf{d}_{\mathrm{s}})}{\partial d_{\mathrm{s}}(i)}\mathbf{C}^{-1}(\mathbf{d}_{\mathrm{s}})\frac{\partial \mathbf{C}(\mathbf{d}_{\mathrm{s}})}{\partial d_{\mathrm{s}}(j)}\right],\ \text{where, } i,j=1,...,K. \quad (13)$$

The CRB of x_{t} and y_{t} are diagonal entries of $\mathrm{CRB}_{\mathbf{u}}$ as

$$\mathrm{CRB}_{x_{\mathrm{t}}}=\frac{\Theta_{\mathrm{b}}}{\Theta_{\mathrm{a}}\Theta_{\mathrm{b}}-[\Theta_{\mathrm{c}}]^{2}}, \quad (20)$$

$$\mathrm{CRB}_{y_{\mathrm{t}}}=\frac{\Theta_{\mathrm{a}}}{\Theta_{\mathrm{a}}\Theta_{\mathrm{b}}-[\Theta_{\mathrm{c}}]^{2}}. \quad (21)$$

The sum of the CRB of coordinates x_{t} and y_{t} is

$$\mathrm{CRB}_{x_{\mathrm{t}},y_{\mathrm{t}}}(\mathbf{x},\mathbf{y})=\frac{\Theta_{\mathrm{b}}+\Theta_{\mathrm{a}}}{\Theta_{\mathrm{a}}\Theta_{\mathrm{b}}-[\Theta_{\mathrm{c}}]^{2}}. \quad (22)$$

Finally, the objective of localization is to minimize $\mathrm{CRB}_{x_{\mathrm{t}},y_{\mathrm{t}}}(\mathbf{x},\mathbf{y})$. Notice that since the exact values of x_{t} and y_{t} are unknown in $\mathrm{CRB}_{x_{\mathrm{t}},y_{\mathrm{t}}}(\mathbf{x},\mathbf{y})$, we use an initial estimation $[\widehat{x}_{\mathrm{t}},\widehat{y}_{\mathrm{t}}]^{T}$ to substitute $\mathrm{CRB}_{x_{\mathrm{t}},y_{\mathrm{t}}}(\mathbf{x},\mathbf{y})$ in problem formulation. Then, the metric is $\mathrm{CRB}_{\widehat{x}_{\mathrm{t}},\widehat{y}_{\mathrm{t}}}(\mathbf{x},\mathbf{y})$.

III. Problem Formulation and Proposed Algorithm

A. Weighted Problem Formulation

We formulate a UAV path design problem by applying a weighting factor η to characterize the trade-off between $\overline{R}(\mathbf{S})$ and $\mathrm{CRB}_{\widehat{x}_{\mathrm{t}},\widehat{y}_{\mathrm{t}}}(\mathbf{x},\mathbf{y})$. The trade-off problem is formulated as

$$\mathrm{P1}:\min_{\{\mathbf{S},\mathbf{x},\mathbf{y},\mathbf{V}\}}\ \eta\cdot\frac{\mathrm{CRB}_{\widehat{x}_{\mathrm{t}},\widehat{y}_{\mathrm{t}}}(\mathbf{x},\mathbf{y})}{\mathrm{CRB}_{\mathrm{norm}}}-(1-\eta)\cdot\frac{\overline{R}(\mathbf{S})}{R_{\mathrm{norm}}}$$

$$\text{s.t. } \|\mathbf{v}_n\|\le V_{\max}, n=1,2,...,N, \quad (23)$$

$$0\le x_n\le L_x, 0\le y_n\le L_y, n=1,2,...,N, \quad (24)$$

$$T_{\mathrm{f}}\cdot\sum_{n=1}^{N}P(\|\mathbf{v}_n\|)+T_{\mathrm{h}}\cdot\sum_{k=1}^{K}P(0)\le E_{\mathrm{tot}}. \quad (25)$$

We normalize the two performance metrics with $\mathrm{CRB}_{\mathrm{norm}}$ and R_{norm}. $\mathrm{CRB}_{\mathrm{norm}}$ is the value of (9) with largest d_{t} and R_{norm} is the date rate with largest d_{c}. $V_{\max}$ is the UAV maximum flying speed. E_{tot} denotes the total on-board energy of the UAV. The power consumption in (25) can be modeled as [18]

$$P(V)=P_0\left(1+\frac{3V^2}{{U_{\mathrm{tip}}}^2}\right)+P_{\mathrm{i}}\left(\sqrt{\left(1+\frac{V^4}{4{v_0}^4}\right)}-\frac{V^2}{2{v_0}^2}\right)^{\frac{1}{2}}+\frac{1}{2}d_0\rho sAV^3. \quad (26)$$

B. Proposed Algorithm

As P1 includes non-convex objective function and constraints, it is unlikely to obtain a globally optimal solution. Here we propose an iterative algorithm to address P1 and seek a locally optimal solution.

We first deal with (25). Since the second term of the left-hand-side (LHS) of (26) is non-convex, we introduce variables $\boldsymbol{\delta}=\{\delta_1,\delta_2,...,\delta_N\}$ to recast this term by relaxing it to an inequality as

$$\delta_n^2\ge\sqrt{\left(1+\frac{\|\mathbf{v}_n\|^4}{4v_0^4}\right)}-\frac{\|\mathbf{v}_n\|^2}{2v_0^2}, \quad (27)$$

$$\delta_n\ge 0. \quad (28)$$

And (27) is equivalent to

$$\frac{\|\mathbf{v}_n\|^2}{v_0^2}\ge\frac{1}{\delta_n^2}-\delta_n^2, n=1,2,...,N. \quad (29)$$

(25) can be rewritten by (28), (29) and the following constraint

$$E_{\mathrm{tot}}\ge T_{\mathrm{h}}\cdot\sum_{k=1}^{K}\{P_0+P_{\mathrm{i}}\}+T_{\mathrm{f}}\cdot\sum_{n=1}^{N}\left\{P_0\left(1+\frac{3\|\mathbf{v}_n\|^2}{{U_{\mathrm{tip}}}^2}\right)+P_{\mathrm{i}}\delta_n+\frac{1}{2}d_0\rho sA\|\mathbf{v}_n\|^3\right\}. \quad (30)$$

(29) can be addressed with SCA algorithm. Specifically, any convex function is globally lower-bounded by its first-order Taylor expansion at any point [19]. We approximate LHS of (29) by its first-order Taylor expansion near a given point as

$$\frac{\|\mathbf{v}_n\|^2}{v_0^2}\ge\frac{\|\mathbf{v}_n^{(l-1)}\|^2}{v_0^2}+\frac{2}{v_0^2}\mathbf{v}_n^{(l-1)}\left(\mathbf{v}_n-\mathbf{v}_n^{(l-1)}\right)^{T}\ge\frac{1}{\delta_n^2}-\delta_n^2. \quad (31)$$

Thus, we find the lower bound for the LHS of (29). As the right-hand-side (RHS) of (29) is still non-convex, we introduce variables $\boldsymbol{\xi}=\{\xi_1,\xi_2,...,\xi_N\}$ and rewrite the RHS of (29) as

$$\frac{1}{\delta_n^2}-\xi_n\ge\frac{1}{\delta_n^2}-\delta_n^2, n=1,2,...,N, \quad (32)$$

$$\delta_n^2\ge\xi_n, n=1,2,...,N, \quad (33)$$

$$\xi_n\ge 0, n=1,2,...,N. \quad (34)$$

We can observe that the newly introduced constraint (33) is non-convex. To tackle this issue, we approximate the LHS of (33) by its first-order Taylor expansion near $\boldsymbol{\delta}^{(l-1)}$ as

$$\delta_n^2\ge\left[\delta_n^{(l-1)}\right]^2+2\delta_n^{(l-1)}\left(\delta_n-\delta_n^{(l-1)}\right)\ge\xi_n, n=1,2,...,N. \quad (35)$$

Finally, the lower bound of the LHS of (29) and the upper bound of the RHS of (29) are revealed. A new constraint to substitute (29) with new variables is obtained as

$$\frac{\|\mathbf{v}_n^{(l-1)}\|^2}{v_0^2}+\frac{2}{v_0^2}\mathbf{v}_n^{(l-1)}\cdot\left(\mathbf{v}_n-\mathbf{v}_n^{(l-1)}\right)^{T}\ge\frac{1}{\delta_n^2}-\xi_n. \quad (36)$$

Through the above process, all constraints in P1 are approximated by convex functions. But P1 is still non-convex because of the non-convex objective term $\mathrm{CRB}_{\widehat{x}_{\mathrm{t}},\widehat{y}_{\mathrm{t}}}(\mathbf{x},\mathbf{y})$. Now, we approximate $\mathrm{CRB}_{\widehat{x}_{\mathrm{t}},\widehat{y}_{\mathrm{t}}}(\mathbf{x},\mathbf{y})$ by its first-order Taylor expansion near given points $\mathbf{x}^{(l-1)}$ and $\mathbf{y}^{(l-1)}$ in (37), where $\nabla\mathrm{CRB}_{x_k}$ and $\nabla\mathrm{CRB}_{y_k}$ represent the gradient of $\mathrm{CRB}_{\widehat{x}_{\mathrm{t}},\widehat{y}_{\mathrm{t}}}(\mathbf{x},\mathbf{y})$ with respect to x_k and y_k respectively.

We rewrite P1 as

$$\mathrm{P1}':\min_{\{\mathbf{S},\mathbf{x},\mathbf{y},\mathbf{V},\boldsymbol{\delta},\boldsymbol{\xi}\}}\ \eta\cdot\frac{F(\mathbf{x},\mathbf{y})}{\mathrm{CRB}_{\mathrm{norm}}}-(1-\eta)\cdot\frac{\overline{R}(\mathbf{S})}{R_{\mathrm{norm}}}$$

$$\text{s.t. (23), (24), (28), (30), (34) and (36).}$$

The solution of $\mathbf{x}$ and $\mathbf{y}$ in P1′ are $\mathbf{x}^*$ and $\mathbf{y}^*$ respectively. In the l-th iteration, $\mathbf{x}^*-\mathbf{x}^{(l-1)}$ and $\mathbf{y}^*-\mathbf{y}^{(l-1)}$ are descent

$$\begin{aligned}
&\mathrm{CRB}_{\widehat{x}_\mathrm{t},\widehat{y}_\mathrm{t}}\left(\mathbf{x},\mathbf{y}\right)\\
&\approx \mathrm{CRB}_{\widehat{x}_\mathrm{t},\widehat{y}_\mathrm{t}}\left(\mathbf{x}^{(l-1)},\mathbf{y}^{(l-1)}\right)+\sum_{k=1}^{K}\nabla\mathrm{CRB}_{x_k}\left(\mathbf{x}^{(l-1)},\mathbf{y}^{(l-1)}\right)\left(x_k-x_k^{(l-1)}\right)+\sum_{k=1}^{K}\nabla\mathrm{CRB}_{y_k}\left(\mathbf{x}^{(l-1)},\mathbf{y}^{(l-1)}\right)\left(y_k-y_k^{(l-1)}\right)\\
&=\mathrm{CRB}_{\widehat{x}_\mathrm{t},\widehat{y}_\mathrm{t}}\left(\mathbf{x}^{(l-1)},\mathbf{y}^{(l-1)}\right)+F\left(\mathbf{x},\mathbf{y}\right). \qquad (37)
\end{aligned}$$

TABLE I
SIMULATION PARAMETERS

parameter	value	parameter	value
P_0	80 W	P_i	88.6 W
U_tip	120 m/s	v_0	4.03 m/s
d_0	0.6	s	0.05 m^3
ρ	1.225 $\mathrm{kg/m}^3$	A	0.503 m^2
α_0	-40 dB	β_0	-39 dB
N_0	-170 dBm/Hz	σ_0^2	$N_0 B$
P	20 dBm	B	1 MHz
G_p	$0.1B$	N	80
V_max	30 m/s	T_f	1.2 s
H	200 m	T_h	1.5 s
V_0	10 m/s	M	4
L_x	2000 m	L_y	2000 m

directions of $\mathbf{x}$ and $\mathbf{y}$ [19]. Next, we use stepsize ω $(0 \leq \omega \leq 1)$ and seek points that are able to obtain the minimum $\mathrm{CRB}_{\widehat{x}_\mathrm{t},\widehat{y}_\mathrm{t}}\left(\mathbf{x},\mathbf{y}\right)$ following the descent direction. The result points are expressed respectively as

$$\mathbf{x}^{(l)}=\mathbf{x}^{(l-1)}+\omega\left(\mathbf{x}^{*}-\mathbf{x}^{(l-1)}\right), \qquad (38)$$

$$\mathbf{y}^{(l)}=\mathbf{y}^{(l-1)}+\omega\left(\mathbf{y}^{*}-\mathbf{y}^{(l-1)}\right). \qquad (39)$$

Since the proposed algorithm above is an iterative process, initial inputs of $x_k^{(0)}$, $y_k^{(0)}$, $\mathbf{v}_n^{(0)}$, $\delta_n^{(0)}$ and $\xi_n^{(0)}$ are needed. Here, we design an initial trajectory and calculate $x_k^{(0)}$, $y_k^{(0)}$, $\mathbf{v}_n^{(0)}$, $\delta_n^{(0)}$, and $\xi_n^{(0)}$ based on the trajectory. We use a straight line from the start point directly to the communication user with a fixed flying speed V_0 as the initial trajectory.

IV. NUMERICAL ANALYSIS

This section provides numerical results to evaluate the performance of our proposed approaches. In the simulation, we set the charging base for the UAV to charge its battery energy at $[x_\mathrm{B},y_\mathrm{B}]^T=[100,100]^T$. The simulation related parameters are shown in Table I.

In Fig. 2 and Fig. 3, we first compare the proposed algorithm performance with different measurement Gaussian noise. In Fig. 2, we use "MSE" to present the MSE of the target coordinates estimate using maximum likelihood estimation (MLE). "CRB" is the value of (22). In Fig. 3, "CRB" denotes the objective function value in P1, and "MSE" denotes that we use MSE to substitute $\mathrm{CRB}_{x_\mathrm{t},y_\mathrm{t}}\left(\mathbf{x},\mathbf{y}\right)$ in P1. In Fig. 2, it is shown that when $a=10$, which means the measurement Gaussian noise with a larger variance, the estimation error increases compared with $a=1$. That is because when the distance measurement has a higher measurement error, a coordinate estimate with higher error occurs. In Fig. 2, we also observe that with E_tot increase, trends of "MSE" and "CRB" are both decreasing. CRB provides a lower bound for the MSE of MLE. The increasing energy realizes a lower estimation error, resulting in a performance improvement for radar sensing. In Fig. 3, it shows that the joint radar sensing and communication performance is improved with the growth of the total energy budget of the UAV.

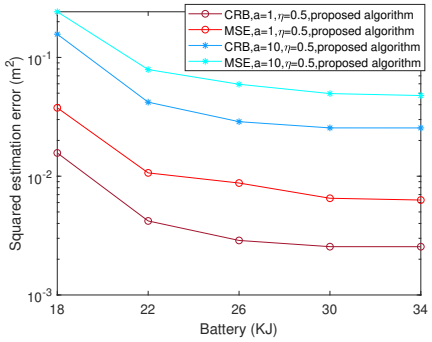

Fig. 2. Sensing performance of different a with an increasing E_tot

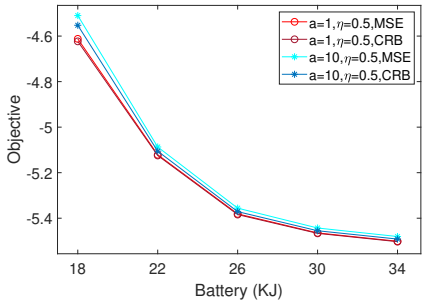

Fig. 3. Objective value of different a with an increasing E_tot

We set $[x_\mathrm{t},y_\mathrm{t}]^T=[380,1600]^T$ and $[x_\mathrm{c},y_\mathrm{c}]^T=[1700,1800]^T$. In Fig. 4 and Fig. 5, we aim to show the performance trade-off between communication and sensing. It can be seen that there exists a trade-off between the average data rate and estimation error. When η increases, that means the CRB value contributes more to the objective, a lower estimation error and a lower average data rate are achieved, i.e. when $\eta=0.7$, the squared estimation error is around $1.5\times10^{-3}\mathrm{m}^2$ and data rate is around 9.4 Mbits/s. On the contrary, a lower η realizes a better communication performance, i.e., when $\eta=0.3$, the squared estimation

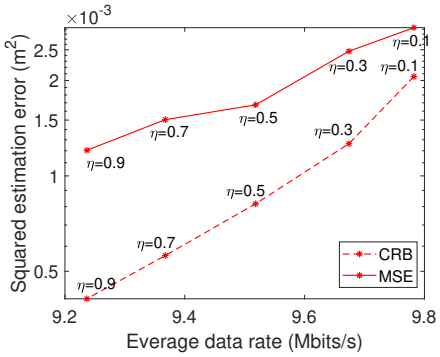

Fig. 4. Trade-off between communication and radar sensing in the proposed trajectory design approach ($E_{\rm tot} = 26$KJ)

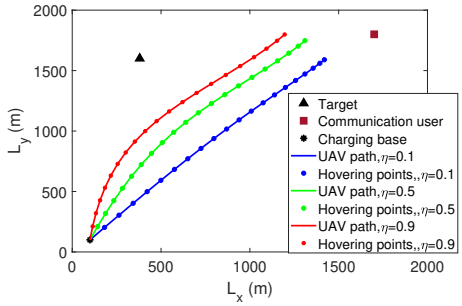

Fig. 5. UAV trajectories of the proposed trajectory design approach with the different weighting factor ($E_{\rm tot} = 26$KJ)

error increases to $2.5 \times 10^{-3}\mathrm{m}^2$ and data rate increases to 9.7 Mbits/s. Fig. 5 shows the UAV paths with different η to explicate the trade-off between communication and sensing. It can be observed that with a larger η, the UAV trajectory is more suitable for it to perform target sensing. For example, the UAV flies closer to the target, so that the sensing can be performed in lower noise environment.

V. Conclusion

In this paper, we have considered a trade-off UAV path design for a UAV based joint radar localization and communication system. Firstly, the CRB is exploited to substitute MSE as the target localization metric. Then, a weighted problem for the UAV path design to achieve a flexible trade-off between radar sensing and communication is formulated. We further developed an iterative algorithm to address the objective and constraints in the path design formulation. The simulations have shown that the UAV battery capacity increase can improve the joint performance in this scenario. The weighting factor can provide a flexible trade-off between the joint performance of communication and radar localization.

VI. Acknowledgment

This paper has received funding from the European Union's Horizon 2020 research and innovation programme under the Marie Sklodowska-Curie grant agreement No 812991.

References

[1] A. Liu *et al*, "A survey on fundamental limits of integrated sensing and communication," *IEEE Commun. Surveys Tuts.*, Apr. 2021.

[2] J. Wang, C. Jiang, Z. Han, Y. Ren, R. G. Maunder, and L. Hanzo, "Taking drones to the next level: Cooperative distributed unmanned-aerial-vehicular networks for small and mini drones," *IEEE Trans. Veh. Technol.*, vol. 12, no. 3, pp. 73–82, Sep. 2017.

[3] Y. Zeng, R. Zhang, and T. J. Lim, "Wireless communications with unmanned aerial vehicles: Opportunities and challenges," IEEE Commun. Mag.,vol. 54, no. 5, pp. 36-42, May, 2016.

[4] A. Al-Hourani, S. Kandeepan, and S. Lardner, "Optimal LAP altitude for maximum coverage," *IEEE Wireless Commun. Lett.*, vol. 3, no. 6, pp. 569–572, Dec. 2014.

[5] B. Li, C. Chen, R. Zhang, H. Jiang, and X. Guo, "The energy-efficient UAV-based BS coverage in air-to-ground communications," in *Proc. IEEE Workshop Sensor Array and Multichannel Signal Process. (SAM Wkshps)*, Jul. 2018, pp. 578–581.

[6] H. He, S. Zhang, Y. Zeng, and R. Zhang, "Joint altitude and beamwidth optimization for UAV-enabled multiuser communications," *IEEE Commun. Lett.*, vol. 22, no. 2, pp. 344-347, Feb., 2018.

[7] M. Mozaffari, W. Saad, M. Bennis, and M. Debbah, "Drone small cells in the clouds: Design, deployment and performance analysis," in *Proc. IEEE Global Commun. Conf. (GLOBECOM)*, Dec. 2015, pp. 1–6

[8] J. Lyu, Y. Zeng, R. Zhang, and T. J. Lim, "Placement Optimization of UAV-Mounted Mobile Base Stations", *IEEE Commun. Lett.*, vol. 21, no. 3, pp. 604-607, Mar., 2017.

[9] K. Doğançay, "Single- and multi-platform constrained sensor path optimization for angle-of-arrival target tracking," in *Proc. Eur. Signal Process. Conf.*, Aug. 2010, pp. 835-839.

[10] Babu, Nithin, et al. "Fairness Based Energy-Efficient 3D Path Planning of a Portable Access Point: A Deep Reinforcement Learning Approach." arXiv preprint arXiv:2208.05265 (2022).

[11] I. Donevski, N. Babu, J. J. Nielsen, P. Popovski and W. Saad, "Federated Learning With a Drone Orchestrator: Path Planning for Minimized Staleness," *IEEE Open Journal of the Communications Society*, vol. 2, pp. 1000-1014, April 2021.

[12] X. Wang, Z. Fei, J. A. Zhang, J. Huang and J. Yuan, "Constrained utility maximization in dual-functional radar-communication multi-UAV networks," *IEEE Trans. Commun.*, vol. 69, no. 4, pp. 2660-2672, April 2021.

[13] K. Zhang and C. Shen, "UAV aided integrated sensing and communications," in *Proc. IEEE Veh. Technol. Conf*, Sept. 2021, pp. 1-6.

[14] F. Liu, W. Yuan, C. Masouros and J. Yuan, "Radar-assisted predictive beamforming for vehicular links: communication served by sensing," in *IEEE Trans. Wireless Commun.*, vol. 19, no. 11, pp. 7704-7719, Nov. 2020.

[15] Steven M. Kay, *Fundamentals of statistical signal processing: Estimation theory*. Upper Saddle River, U.S.: Prentice Hall, 1993, pp. 15-67.

[16] M. A. Al-Jarrah, A. Al-Dweik, Emad Alsusa and E. Damiani, "RFID Reader Localization Using Hard Decisions With Error Concealment," *IEEE Sensors Journal*, vol. 19, no. 17, pp. 7534-7542, Sept.1.

[17] Steven.M.Key, *Fundamentals of statistical signal processing, volume II: Detection theory*. Upper Saddle River, U.S.: Prentice Hall PTR, 1993, pp. 20-36.

[18] Y. Zeng, J. Xu, and R. Zhang, "Energy minimization for wireless communication with rotary-wing UAV," *IEEE Trans. Wireless Commun.*, vol. 18, no. 4, pp. 2329 - 2345, Apr. 2019.

[19] S. Boyd and L. Vandenberghe, *Convex optimization*. Cambridge, U.K.: Cambridge Univ. Press, 2004.